Optimized synthesis of nano-scale high quality HKUST-1 under mild conditions 1 and its application in CO2 capture

Mu, X., Chen, Y., Lester, E., Wu, T

University of Nottingham
UK | CHINA | MALAYSIA

University of Nottingham Ningbo China, 199 Taikang East Road, Ningbo, 315100, China

First published 2018

This work is made available under the terms of the Creative Commons Attribution 4.0 International License:
http://creativecommons.org/licenses/by/4.0

The work is licenced to the University of Nottingham Ningbo China under the Global University Publication Licence:

https://www.nottingham.edu.cn/en/library/documents/research-support/global-university-publications-licence.pdf

University of Nottingham
UK | CHINA | MALAYSIA

Optimized synthesis of nano-scale high quality HKUST-1 under mild conditions and its application in CO_2 capture

Xueliang Mu[1,2], Yipei Chen[1,3], Edward Lester[3], Tao Wu[1,2,*]

[1]New Materials Institute, The University of Nottingham Ningbo China, Ningbo 315100, P. R. China

[2]Municipal Key Laboratory of Clean Energy Conversion Technologies, The University of Nottingham Ningbo China, Ningbo 315100, P. R. China

[3]Department of Chemical and Environmental Engineering, The University of Nottingham, Nottingham NG7 2RD, P. R. China

* Corresponding author: Tao.Wu@nottingham.edu.cn

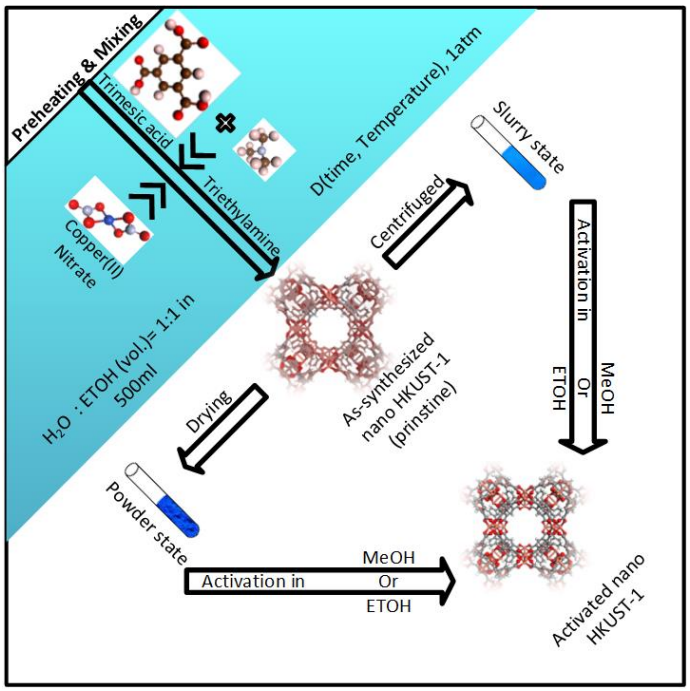

Highlights

- A fast and efficient method was developed for the synthesis of HKUST-1
- Synthesis was conducted under low temperature and atmospheric pressure
- The MOFs was synthesized in nano-scale with high BET surface area and high yield
- Activation agent has shown significant influence on BET surface area of the MOFs
- The HKUST-1 prepared shows excellent CO_2 uptake capacity

Abstract

This study was focused on the development of an optimized method for the rapid synthesis of nano-scale HKUST-1 with high yield, high surface area and high CO_2 uptake capacity but under mild conditions. A series of HKUST-1 were synthesized under different conditions, such as preparation time, temperature, activation method, etc. It was found that the nano-scale HKUST-1 MOFs (T85-3-Pm4-120) was successfully synthesized at a high yield (87%) under low temperature (85°C) using a mixture of Triethylamine(TEA), Cu^{2+} and trimesic acid (TMA) with a molar ratio of 6:3:2. The highest porosity was achieved via this pristine HKUST-1 being activated (powder activation, drying at 120 ^{o}C) four times using methanol to remove impurities trapped in the pores. The best HKUST-1 MOFs (T85-3-Pm4-120) hereby prepared was then tested in CO_2 adsorption and exhibited an adsorption capacity of 2.5 mmol/g. It is therefore demonstrated that the new approach proposed in this study is a rapid and effective way to synthsize highly porous HKUST-1 MOFs under mild conditions, which is of comparable surface area and CO_2 uptake capacity with those MOFs prepared under harsh conditions.

Keywords:

HKUST-1, nano scale, fast synthesis, mild synthesis condition, CO_2 adsorption

1. Introduction

Metal–organic frameworks (MOFs) are hybrid crystalline compounds consisting of organic ligands bridging inorganic moieties. MOFs exhibit unique structure and outstanding properties in porosity, pore size and surface area and have been used in various fields such as gas storage, adsorption, separation, and catalysis[1]. Recently, more and more effort has been made to explore the application of nano-scale MOFs in areas, such as liquid phase catalysis[2-3], adsorption[4] and drug delivery[5], etc.

HKUST-1, a copper-based MOF, is one of the first reported MOFs[6] whose structure is based on Cu^{2+} ions linked with 1,3,5-benzenetricarboxylate struts. The conventional solvothermal method for the preparation of HKUST-1 involves heating the solution up to 180 °C to form crystalline $Cu_3(BTC)_2$ [7]. The $Cu_3(BTC)_2$, synthesized at 75–120 °C, has to be kept in an autoclave for a long period, varying from 1 day up to a few weeks, to remove impurities that are trapped in the pores [8]. Although slow diffusion techniques require significantly long time for the synthesis of MOFs, it is still the preferred method for the synthesis of MOFs due to its tunable reaction conditions, such as, the control of the rate of nucleation and crystal growth by the control of concentration gradient (temperature gradient)[9-13]. Normally, the synthesis of MOFs with good thermal stability has to be conducted under hydro/solvothermal conditions. To date, commonly adopted methods for the rapid preparation of HKUST-1 include microwave heating, ultrasound irradiation, mechanochemistry, and solvothermal synthesis, which are summarized in Table 1. Normally, conventional solvothermal and electrochemical methods require long time to synthesize HKUST-1 with high surface area. Although mechanochemical, microwave heating and ultrasound irradiation methods can be used to produce HKUST in much shorter time, the surface area of the MOFs prepare is not high enough (<1500 m^2/g). In addition, the size of HKUST-1 particles prepared via these methods is in micron scale and cannot meet some special requirements in catalysis when nano particles are preferred to enable higher mass transfer rate or to achieve higher thermal resistance [14-15]. Because of this, there has been numerous work being carried out on the synthesis of nanoscale MOFs [16-18]. However, there is still a need to develop cost-effective techniques for the preparation of nanoscale HKUST-1 MOFs under mild conditions, which are able to produce MOFs with high surface area (>1500 m^2/g).

65 **Table 1 MOFs prepared under Different Methods**

Method	Microwave heating[19]	Ultrasound irradiation[19]	Mechano-chemical[20]	Conventional solvothermal[21]	Electro-chemical[22]
Surface area (m^2/g)	1080	1156 [19]	1421	1000-1800	1500-2100*
Particle Size (µm)	10	0.2-0.4	>50 [a]	1.5–3.5	15.9*
Temperature (°C)	140	25-40	-	100-180	-
Synthesis Time (min)	60	1	20	720-4320	150

66 * Basolite C300, Sigma-Aldrich. [a] from SEM image[20]

67 In this study, the effort was made to develop and optimize a new method for the preparation of
68 HKUST-1 MOFs in a fast and efficient manner. Attempts were also made to control the MOFs in
69 nanoscale with high surface area and high yield. The preparation conditions were optimized to
70 enable the preparation of nanoscale HKUST-1, which was further studied to show its potential in
71 CO_2 capture.

72 **2. Experiment**

73 2.1. Preparation of HKUST-1

74 In this study, a novel hydro/solvo-thermal method was developed for the rapid preparation of
75 porous HKUST-1 MOFs. Firstly, 0.03 mole of copper nitrate trihydrate (Sigma Aldrich, 98%) was
76 dissolved in a 250 ml of deionized water to form Solution A, while 0.02 mole of trimesic acid (TMA)
77 (Sigma Aldrich, 95%) and 0.06mol Triethylamine (TEA) (Sigma Aldrich, 99.8%, anhydrous) were
78 added in a 250 ml of ethanol (Sigma Aldrich, 99%) to form Solution B. These two solutions were
79 then mixed and heated under constant stirring to the pre-set temperature level, i.e., 25, 50, 75,
80 80, 85°C, and kept isothermal for a period of time (3, 6 or 9 h). The solution was then cooled
81 down to room temperature in an ice bath and centrifuged to produce pristine HKUST-1, which
82 was activated using slurry state activation, powder state activation or slurry-powder state

83 activation to remove internal impurities. The slurry state activation refers to the activation of the
84 centrifuged HKUST-1 after synthesis; the powder state activation refers to activation of the dried
85 centrifuged HKUST-1; while the slurry-powder state activation refers to the slurry state activation
86 followed by drying and further activation of the HKUST-1 powder. In this research, the activation
87 agents used are ethanol and methanol. The activation process was performed in a reflux
88 condenser. The amount of ethanol or methanol used was kept at the same level as 62.5 ml per
89 gram of pristine HKUST-1. The activation process was conducted for 3 h. After that, the activated
90 solution was centrifuged to obtain precipitation and dried at 120 ^{o}C to obtain final HKUST-1
91 powder. The sample being activated by slurry/powder state activation method using
92 ethanol/methanol as the agent is denoted as Se/Pe or Sm/Pm ('S and P' stands for slurry state
93 and powder state, while 'e and m' stands for ethanol and methanol). A suite of samples was
94 screened under different conditions, such as reaction period (3, 6, and 9 h), reaction temperature
95 (25, 50, 75, 80, 85°C), activation methods, and drying temperature (120 or 180 ^{o}C)and are named
96 as based on preparation conditions. For example, T85-3-Sm1Pm1-120 stands for a HKUST-1 being
97 prepared under 85 ^{o}C for 3 hour, followed by firstly slurry state activation with methanol as the
98 agent and drying at 120 ^{o}C using an air dryer, and then undergoing powder activation using
99 methanol as the agent followed by drying at 120 ^{o}C.

100 2.2. Characterization

101 Morphology and particle size of the synthesized HKUST-1 MOFs were analyzed by using a
102 Scanning Electron Microscope (SEM, ZEISS Sigma VP/Oxford Instruments). The high quality SEM
103 images, which show around 100 particles, were processed using ImageJ to find out particle size
104 distribution (particle size is determined based on the Feret's dimension). Structure of the solid

phase and crystallinity were analyzed by using a Powder X-ray diffraction (XRD) with a scanning rate of 0.02°/s (2θ) using monochromatic CuK_{α} radiation (Bruker D8 A25) at 40kV and 35mA. The surface area (Brunauer–Emmett–Teller, BET) and pore size of the HKUST-1 were measured using a Micromeritics Tristar 3020 following the method described elsewhere [23]. Thermal decomposition behavior was studied using a thermogravimetric analyzer (TGA, NETZSCH STA49 F3),which involved the heating of the sample from 35 to 900 °C at a heating rate of 10 °C/min under N_2 atmosphere [24]. The pH value of the solution was measured by using a METTLER TOLEDO pH analyzer (FiveEasy Plus- FE28). The crystallinity of each sample was studied to distinguish any possible variation of the crystal pattern. The crystallinity percentage (%C) was defined as the ratio of the sum of the relative intensity of the five most intense peaks and can be calculated using Eq.(1) [25].

$$\%\mathrm{Crystallinity} = \frac{\sum_{i=1}^{5} I_{relsample}}{\sum_{i=1}^{5} I_{relsample\ of\ reference}} \times 100 \qquad \text{(Eq. 1)}$$

In this calculation, the C300 (C300 is commercial product acquired from Sigma) was used as the reference (100% crystallinity).

- CO_2 adsorption testing

CO_2 adsorption was conducted in a TGA system (NETZSCH STA49 F3) following the procedures adopted by others[26]. Initial treatment of the activated sample was carried out in N_2 at 150 ^{o}C for 12 h. The adsorption was carried out using ultra purity CO_2 and N_2 (99.999%). A gas mixture of 133 mL/min of CO_2, 100 mL/min of N_2 and 100 mL/min of protective gas (N_2) was introduced into the sample chamber. Temperature and pressure of the adsorption chamber was maintained at 27 ^{o}C and 1 bar, respectively.

126 CO_2 isotherm of the HKUST-1 MOFs at 27 ^oC was obtained using the Micromeritics ASAP 2020.
127 The degas of the activated sample was conducted at 150 °C for 12 h. The adsorption pressure
128 varied from 2.7 mbar to 1100 mbar, as described elsewhere[27].

129 The CO_2 and N_2 adsorption–desorption cycle at 27°C was obtained using the TGA. Approximately
130 10 mg HKUST-1 MOFs was pre-treated at 150°C for 2 h in a nitrogen environment. The
131 adsorption-desorption cycle was carried out at a flowrate of 60 mL/min of CO2 (99.999%) gas
132 and 40 mL/min of N2 (99.999%), respectively.

133 **3. Results & Discussion**

134 **3.1. Screening synthesis of HKUST-1**

135 In this study, the effect of synthesis temperature, time, pretreatment temperature and activation
136 methods on the synthesis of HKSUT-1 MOFs was investigated. The first attempt was made to find
137 out an optimal reaction duration and temperature for the synthesis of MOFs. From Fig. 1, it can
138 be seen that the variation in reaction time from 3 h to 9 h showed no significant impact on the
139 specific surface area for samples in Region I. That means 3 hours provide sufficient time to allow
140 the synthesis reaction to complete, which is shorter than the time required for conventional
141 HKUST-1 synthesis ($\geqslant$24h)[21]. This is due to the addition of the alkaline TEA, wich is consistent
142 with the finding that the alkaline TEA could accelerate the deprotonation of H_3BTC and promote
143 the nucleation of particles into nanoscale[28]. Furthermore, in Region II, the pristine HKUST-1 had
144 gone through the pretreatment in an air dryer under two different temperatures, 120 and 180
145 ^oC. The results indicated that 120^oC does not have a negative effect on the pores in the HKUST-1.

146 It can be seen from Fig. 1 that in Region III, the two samples prepared at 50 and 85°C showed
147 significantly different BET surface areas. It is obvious that 85°C favors the formation of HKUST-1
148 with large BET surface area. This low temperature (85°C) is much lower than the temperature
149 (180 °C) adopted for the synthesis of HKUST-1 MOFs by Chui et al.[7] The low temperature level
150 can inhibit the formation of the by-product (Cu_2O) and therefore contribute to a high selectivity
151 and yield.

152 After synthesis, the pristine HKUST-1 has to be activated to remove the impurities (unconverted
153 reactant or byproduct) that are trapped in the pores. The activation can also activate the metal
154 sites, which are always surrounded by water and other gas molecules. As shown in Region IV,
155 pristine HKUST-1 was activated via either slurry state or powder state activation by ethanol or
156 methanol. The BET surface area of T85-3-Se1-120 and T85-3-Pe1-120 was lower than that of T85-
157 3-Sm1-120 and T85-3-Pm1-120. It is reported that that methanol is a better activation agent and
158 can remove more impurities than ethanol[29]. It is clear that the BET surface area of T85-3-Pe1-120
159 and T85-3-Pm1-120 was higher than that of T85-3-Sm1-120 and T85-3-Pe1-120, which suggests
160 that powder state activation is more efficient in the removal of impurities from pores.

161 In Region V, it shows that repeated slurry activation resulted in lower BET surface area, which
162 might be due to the destruction of micropores to form larger pores and subsequently result in
163 lower BET surface area. However, repeated powder state activation shows different impacts on
164 BET surface area, as shown in Region VI. Four times of powder state activation result in the
165 highest surface area around 1542.4 m^2/g.

The combination of slurry-powder state activation was applied to activate pristine HKUST-1 and the BET surface area of individual samples is shown in Region VII in Figure 1. It is found that the BET surface area of T85-3-Sm1Pm1-120, T85-3-Se1Pm1-120 and T85-3-Sm1Pe1 was higher than that of their respective samples being activated once via slurry state activation. For example, T85-3-Sm1Pm1-120 has a BET surface area of 1264.6 m^2/g, which is higher than that of T85-3-Sm1-120 (954.4 m^2/g). In addition, it was found that the BET surface area of T85-3-Sm1Pm1-120 was higher than that of T85-3-Sm1Pe1-120 (1022.7 m^2/g), which again proves the powder state activation using methanol as the activation agent is a reliable and efficient method. However, the BET surface area of one more times of powder activation by methanol (T85-3-Sm1Pm2-120) was reduced. Therefore, it can be concluded that slurry state activation removes the impurities in the pores but does not significantly contribute to the formation of higher BET surface area.

Among the 17 samples prepared, the highest BET was found for T85-3-Pm4-120, which is 1542.4m^2/g. There are also other five samples, i.e., T85-3-Pm1-120, T85-3-Pm2-120, T85-3-Pm3-120, T85-3-Pm5-120, and T85-3-Sm1Pm1-120, that have BET surface area greater than 1100 m^2/g. The highest BET surface area is attributed to the cleaning of pores, which is associated with a final HKUST-1 yield of 67%.

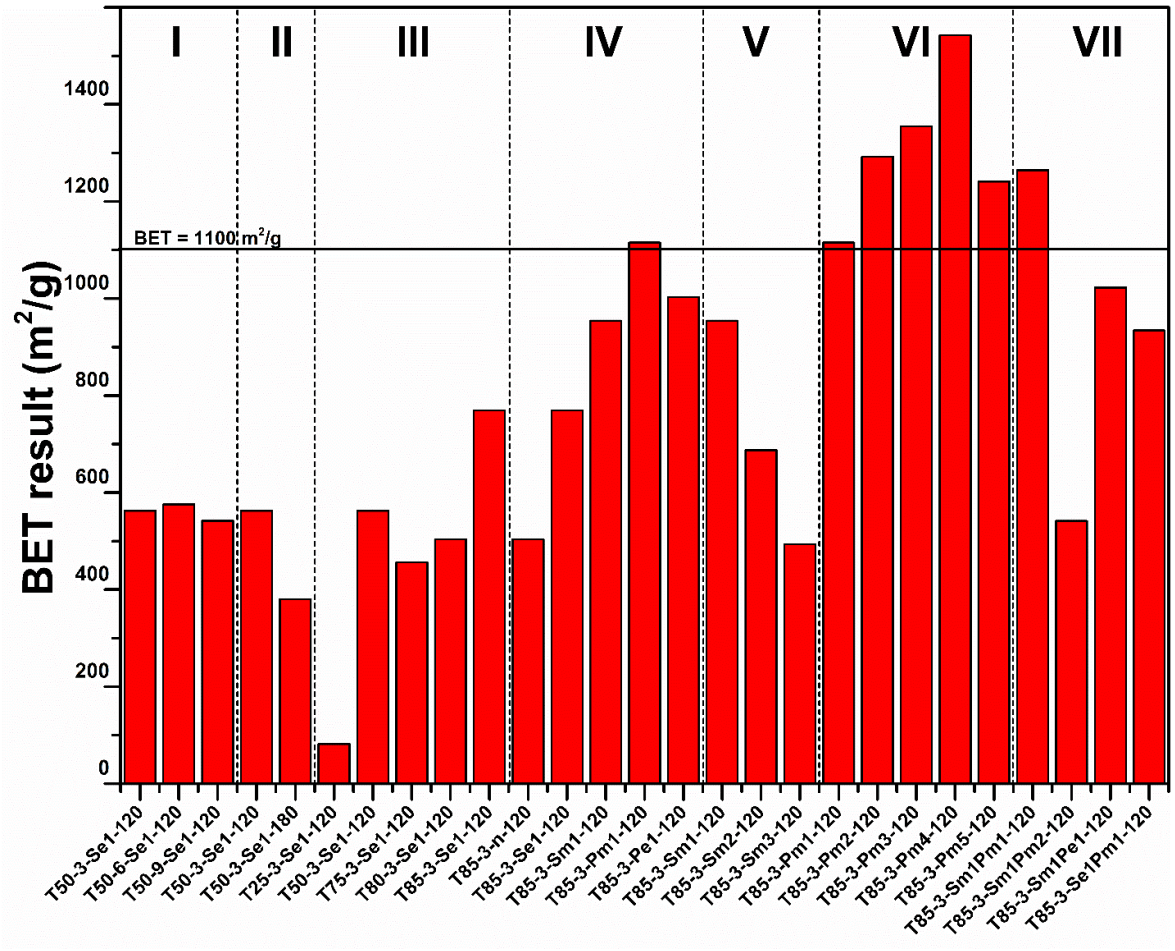

Fig. 1 Screening of HKUST-1 with large specific surface area. I, reaction period; II, Drying temperature; III, synthesis temperature; IV, slurry/powder state activation using methanol/ethanol as the activation agent; V, repeated slurry state activation using methanol as the activation agent; VI, repeated power state activation using methanol as the activation agent; VII combination of slurry and powder activation. (T25, T50, T75, T80, T85-A stand for reaction temperature at 25, 50, 75, 80, 85°C. T50-3, T50-6, T50-9 stand for reaction duration of 3, 6, and 9 h at 50°C, respectively. T50-3-Se1-180 indicate the pristine HKUST-1 yielded at 50°C with a duration of 3 h was activated once using slurry state activation method and dried at 180°C. Sm1 means slurry state HKUST-1 was washed by using methanol. Pe1 means powder state

192 HKUST-1 was washed by using ethanol once. Sm1Pm1 means slurry state washing firstly, and
193 then followed by powder state washing.)

194 **3.2. The nano HKUST-1 formation and its morphological features**

195 To understand how the morphology of HKUST-1 is affected by synthesis conditions and powder
196 activation process, SEM analysis was conducted with morphological features of different samples
197 shown in Fig. 2 (I) – (IV). It is evident that all samples are of nano-particle size (<100 nm) but form
198 agglomerates. In the Region I of Fig. 2 and Fig. 3, the samples synthesized under 50 ^{o}C for 3/6/9h
199 were similar in morphology, but particle size of the samples decreased with the increase in
200 synthesis period. That means longer synthesis period favors the formation of smaller nanoscale
201 particle.

202 Regarding the influence of synthesis temperature on the morphology of HKUST-1, as shown in
203 Region II of Fig. 2 and Fig. 3, the samples synthesized from 25 to 85°C after 3 h demonstrated
204 differences in particle size distribution and average particle size. The SEM image (Fig. 2(II)) shows
205 similar morphology, which are featured with small spherical particles. Under low temperature
206 (25°C), it shows crystal structure with blocky shape and obvious sharp edges and has the highest
207 average particle size of 93.6 nm, whereas samples prepared under higher temperatures
208 (50 ,75 ,85°C) are more spherical and are of smaller particle size. It was obvious that the MOFs
209 prepared at 50 ^{o}C and 85°C formed are of similar average particle size (~72 nm) as shown in the
210 Region II of Figure 3(b). However, the peak (53.8-67.5 nm) of T85-3-Se1-120 is higher than the
211 peak (67.5-87.2 nm) of T50-3-Se1-120 in the Region II of Figure 3(a).

212 In this study, further investigation was conducted to understand the influence of powder
213 activation and slurry activation process on the samples prepared under the optimal synthesis
214 temperature of 85°C. It was found that when the pristine sample had undergone powder
215 activation using methanol as the activation agent twic, the average particle size was the smallest
216 (76.0 nm) with the peak of particle distribution in the range of 67.5-81.25nm. However, the
217 particle size increased when the sample had undergone more times of powder state activation,
218 which could be attributed to the crystal growth of the primary particle during the activation
219 process, i.e., the precursors being washed out of the pores to form new MOFs on the surface of
220 the primary MOF particle.

221 For comparison purpose, the slurry state activation using methanol as activation agent was also
222 conducted. The samples, T85-3-Sm**X**-120 (X=1, 2, 3), were prepared and are shown in Fig. 2(III).
223 These samples showed different morphologies and demonstrated that particle size can be
224 reduced followed by the additional times of slurry state activation, which is shown in the Fig. 3a
225 (III). It can be seen from Fig. 3b (III) and (IV) that slurry state activation leads to the formation of
226 samples with samller particle size a compared with powder state activation. However, although
227 slurry activation process can lead to the formation of smaller size nano particles, it cannot form
228 nano-scale HKUST-1 particle with BET surface area greater than 1100 m^2/g (as shown in Region
229 V of Fig. 1). Despite the increase in particle size after 3 times of powder state activation, the
230 specific surface area of T85-3-Pm**X**-120 (X=1, 2, 3, 4) increased from 1115.3 to 1542.4m^2/g as a
231 result of multiple powder state activations. Therefore, it can be concluded that to form nanoscale
232 sample with large surface area, the sample shall be prepared under 85°C and activated via
233 powder state activation for at least two times.

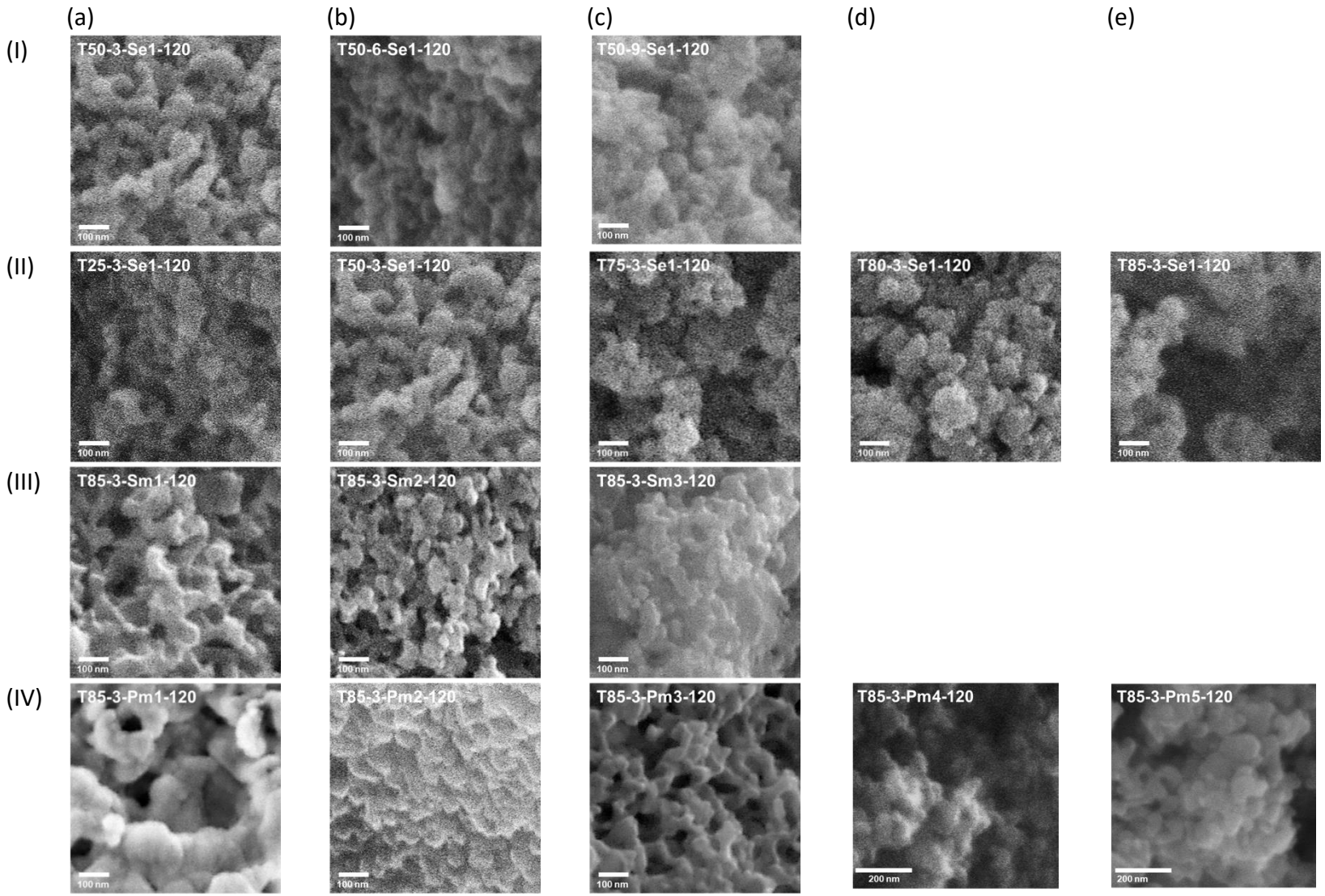

Fig. 2 Morphology of HKUST-1 MOFs prepared under different preparation conditions. I, reaction time. II, synthesis temperature. III, slurry state activation. IV, powder state activation.

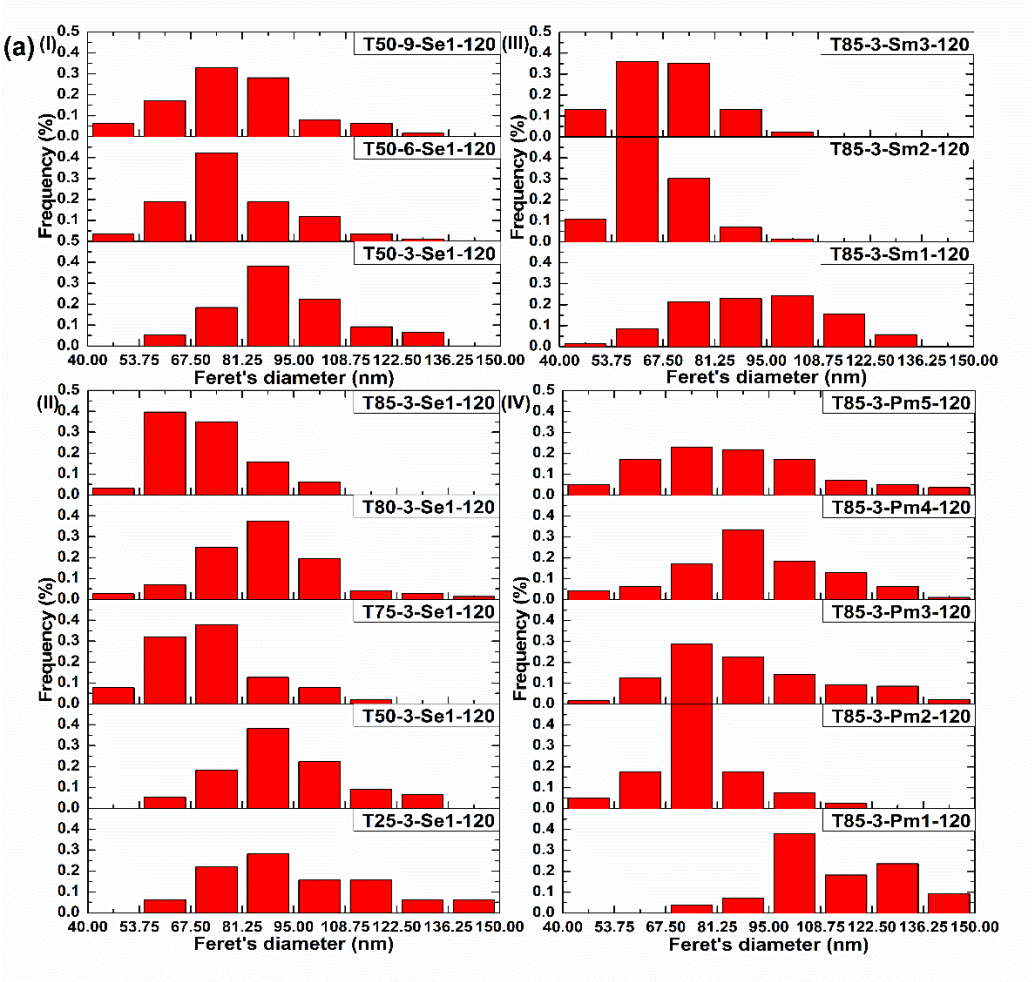
(a)
(I)
T50-9-Se1-120
T50-6-Se1-120
T50-3-Se1-120
(II)
T85-3-Se1-120
T80-3-Se1-120
T75-3-Se1-120
T50-3-Se1-120
T25-3-Se1-120
(III)
T85-3-Sm3-120
T85-3-Sm2-120
T85-3-Sm1-120
(IV)
T85-3-Pm5-120
T85-3-Pm4-120
T85-3-Pm3-120
T85-3-Pm2-120
T85-3-Pm1-120
Frequency (%)
Feret's diameter (nm)
40.00 53.75 67.50 81.25 95.00 108.75 122.50 136.25 150.00

239

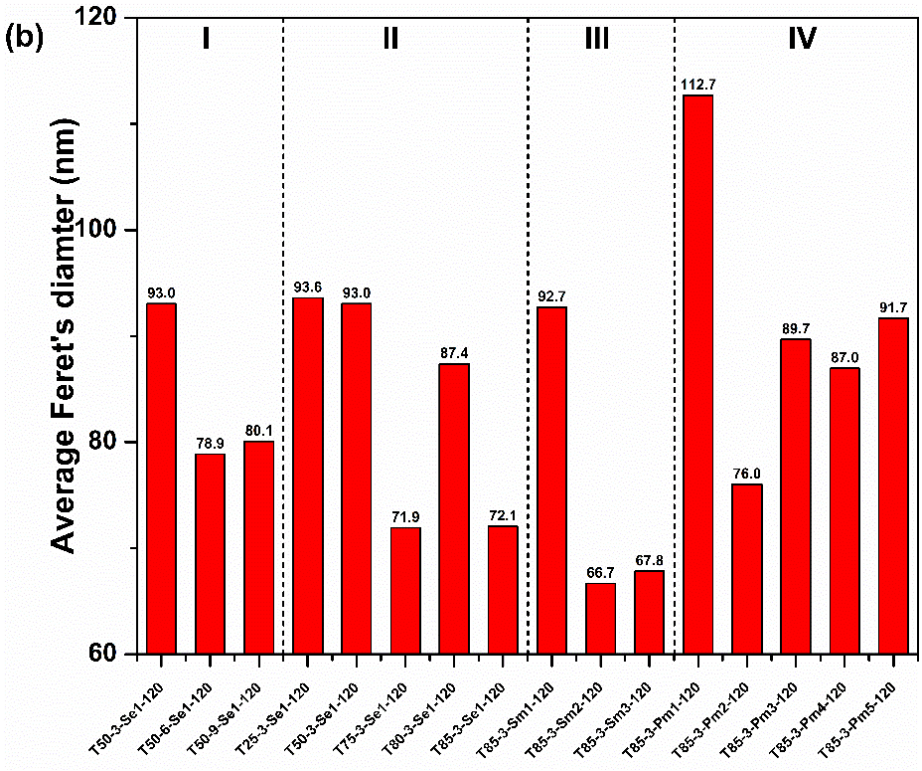

Fig. 3 Particle size (based on Feret's diameter) of each synthesized sample vs different preparation method (results obtained from ImageJ). a, particle size distribution. b, average particle size (average Feret's diameter). I, reaction time. II, synthesis temperature. III, slurry state activation process. IV, powder state activation.

Table 2 Structural properties of samples prepared under 85°C

PREPARATION METHOD	S_{BET}[1] (m^2/g)	$S_{LANGMUIR}$[2] (m^2/g)	$V_{TOTAL\ PORE}$[3] (cm^3/g)	$V_{MICRO\text{-}PORE}$[4] (cm^3/g)	$\%V_{MICRO\text{-}PORE}$[5] (cm^3/g)	pH*
T85-3-N-120	503.5	580.1	0.31	0.20	0.65	3.63
T85-3-Se1-120	769.6	904.7	0.58	0.29	0.50	3.60
T85-3-Sm1-120	954.4	1197.7	0.49	0.40	0.82	3.86
T85-3-Pm1-120	1032.3	1235.4	0.55	0.45	0.82	7.01
T85-3-Pe1-120	1003.0	1161.1	0.47	0.38	0.81	6.07
T85-3-Sm2-120	687.5	719.7	0.49	0.23	0.47	4.78
T85-3-Sm3-120	493.5	516.4	0.36	0.16	0.44	5.63

T85-3-Pm2-120	1292.3	1452.4	0.56	0.47	0.84	7.70
T85-3-Pm3-120	1354.6	1579.3	0.63	0.54	0.86	7.87
T85-3-Pm4-120	1542.4	1647.9	0.65	0.57	0.88	8.17
T85-3-Pm5-120	1241.0	1358.2	0.53	0.46	0.87	8.20
T85-3-Sm1Pm1-120	1264.6	1437.8	0.57	0.49	0.86	6.22
T85-3-Sm1Pm2-120	541.6	731.2	0.45	0.24	0.53	6.88
T85-3-Sm1Pe1-120	1022.7	1184.5	0.48	0.40	0.83	6.18

Note:1. Specific surface area by BET. 2. Specific surface area by Langmuir. 3. Total pore volume by original Horvath-Kawazoe. 4. Micro pore volume by t-plot. 5. Micro pore volume percentage in total volume. * pH values of solution were measured after activation.

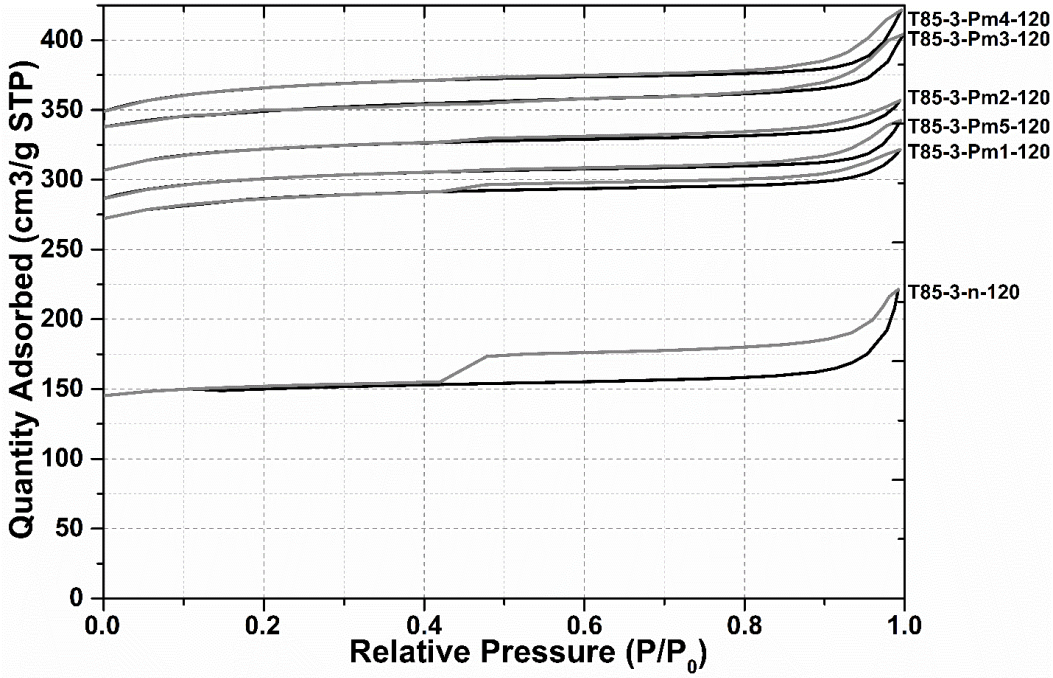

Fig. 4 Nitrogen adsorption and desorption isotherms of the synthesized HKUST-1. For each sample, top line is the adsorption isotherm, bottom line is the desorption isotherm.

3.3. Nitrogen isotherm analyses

It is found that N_2 adsorption rate increases at a low relative pressure ($0.0< P/P_0<0.1$) (as shown in Fig. 4), the shape of each line indicates that they are Type I isotherm according to the IUPAC (International Centre for Theoretical and Applied Chemistry) classification [26, 30]. Samples with Type I isotherm are of microporous (<2nm) structure [31]. The hysteresis loop at a higher relative pressure ($P/P_0>0.4$) indicates capillary condensation of mesopores for N_2, which contributes to the stacking combination of large particle of HKUST-1[32] or the creation of defects under such synthesis method [33]. That is, the hysteresis loop for T85-3-n-120 and T85-3-Pm1-120 would be due to the defects, because this loop was the cavitation phenomenon[34] that occurs when the pore size is less than 6 nm. Besides, the hysteresis loop for T85-3-Pm**X**-120 (X=2,3,4,5) at P/P0 > 0.8 appeared due to larger pores over 10 nm [35]. This loop is caused by the interparticle pores of nanoparticle agglomerate[36].

The influence of activation process on the surface properties of HKUST-1 was also investigated in this study. As shown in Table 2, BET surface area after activation is in the range of 503-1542 m^2/g, which is very close to the values reported by Diring [37] and Ameloot[38], but much higher than those obtained by Chui[7]. Regarding total pore volume, the reported values are in the range of 0.21 - 0.79 cm^3/g [39], whereas the effective pore volume was reported as 0.82 cm^3/g [40]. In this study, the as-synthesized samples exhibited a total pore volume of 0.31-0.65 cm^3/g, which is comparable with reported data. The relatively low N_2 adsorption capacity of the raw material (T85-3-N-120) is attributed to some micropores being blocked by TEA and/or its derivatives. The high N_2 adsorption capacity indicates that the modulator is absent from the pores after activation. The percentage of micropore volume shown in Table 2 suggests that these samples are comprised of

274 plenty of micropores. It can be seen from Table 2 that activation process (powder, slurry and
275 combination activation) has significant influences on pore properties (BET, Langmuir, Total pore
276 volume, Micropore volume, and Microporosity). As for slurry activation, both methanol and
277 ethanol can be used as the agent to clean the interior of pore and therefore improve N_2
278 adsorption capacity. However, more times (>2) of slurry state activation using methanol as the
279 activation agen would result in smaller BET surface area. This is associated with the decrease in
280 the percentage of micropores, which means excessive times of slurry state activation might
281 damage micropores and form more mesopores.

282 As showin in Table 2, the slurry state activation followed by power state activation once led to
283 the formation of HKUST-1 with better pore properties. However, powder state activation is more
284 effective in the removal of impurities trapped in pores and multiple powder state activation could
285 result in high BET surface area (T85-3-PM4-120, 1542.4m^2/g).

286 Meanwhile, the pH value of the solution after activation was monitored by using a pH meter, the
287 results of which are shown in Table 2. It is clear that pH value generally increased with BET specific
288 surface area, which is associated with the removal of impurities and TEA derivatives. It is
289 speculated that powder state activation retained the high BET surface area and did not damage
290 the pore structure of HKUST-1. Therefore, the powder state activation by methanol is considered
291 as an appropriate method for the treatment of the pristine HKUST-1.

292 ***3.4. XRD analysis***

293 XRD analysis was conducted to show the crystalline phases of the porous HKUST-1. It can be seen
294 that all the diffraction peaks in Fig 5 (a) and (b) match well with the pattern of C300 and

295 simulation, indicating that these samples are pure phase of HKUST-1. From Fig 5, it is evident that
296 the XRD peak positions and relative intensities of the synthesized MOFs also agree well with those
297 of the simulated HKUST-1 (red spikes labelled by star at the bottom of Fig. 5)[41]. Due to the low
298 temperature condition adopted for the synthesis of HKUST-1, the diffraction peaks of Cu_2O (36.7
299 ^{o}, PDF#04-003-6433) do not show in the XRD spectrum, which means that (Cu_2O) was not formed.

300 It can be seen from Table 3 that the synthesis temperature has significant impacts on the
301 crystallinity of the samples. In the samples of T**X**-3-Se1-120 (X=25, 50, 75, 80, 85), the crystallinity
302 percentage of T85-3-Se1-120 is very close to that of the C300 (%Crystallinity=95.4%), which
303 demonstrates that the low synthesis temperature (85°C) can lead to the formation of HKUST-1
304 with appropriate crystal structure. After the samples were further processed via powder state
305 activation, the crystallinity percentage of each sample did not vary significantly compared with
306 the variation in temperature. The crystallinity percentage is improved until 5 times of powder
307 state activation. However, further powder state activation does not show much influence on
308 crystallinity percentage. Therefore, to obtain the highest crystallinity percentage of HKUST-1, the
309 sample shall be prepared under 85°C with the four times of powder activation process.

310 In addition, the hydration degree of the HKUST-1 could be determined by the I_{200}/I_{220} ratio[42].
311 where higher I_{200}/I_{220} ratio indicates a smaller hydration degree. Normally, a smaller hydration
312 degree indicates that more copper coordination sites are accessible for other molecules, such as
313 CO_2. The T85-3-Pm4-120 shows the highest value of I_{200}/I_{220}, which suggests that it can capture
314 more CO_2 than any other samples. This result suggests that the proper condition (T85-3-Pm4-120)
315 lead to the formation of HKUST-1 with desired properties in CO_2 adsorption.

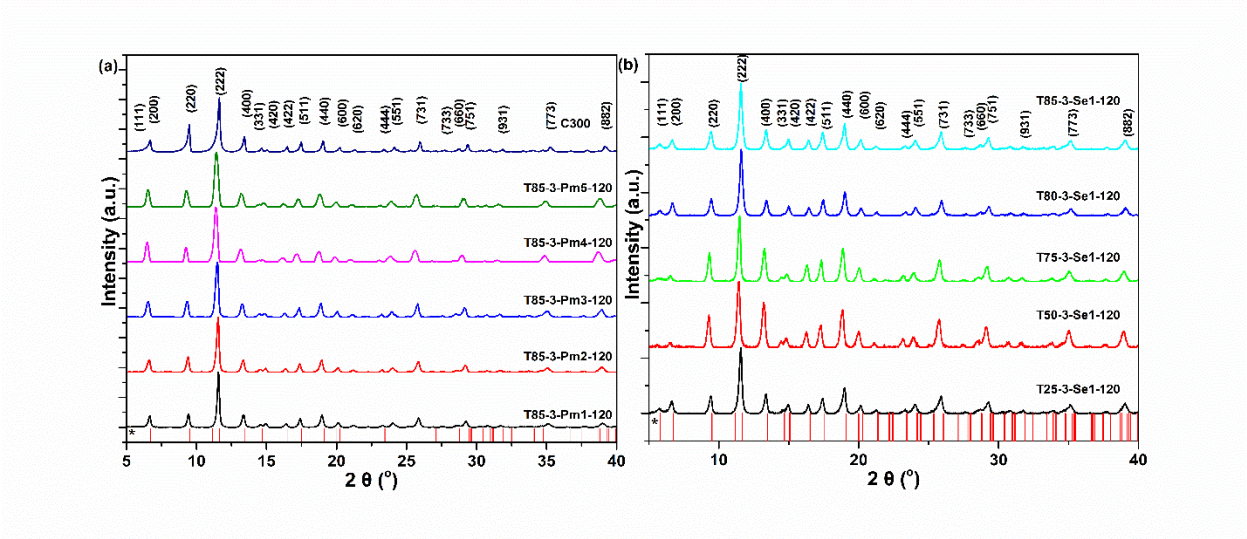

Fig. 5 XRD spectrum of each sample. (a) HKUST-1 activated by repeated powder state activation. (b) HKUST-1 synthesized under different reaction temperatures. * indicates simulated PXRD data from single crystal data.

Table 3 XRD patterns of relative peak intensity based on the HKUST-1 peak intensity of (222)

	$I_{(200)}$ %	$I_{(220)}$ %	$I_{(222)}$ %	$I_{(400)}$ %	$I_{(420)}$ %	%Crystallinity	$I_{(200)}/I_{(220)}$
T85-3-Pm5-120	30.2	30	100	24.0	7.4	98.3	**1.01**
T85-3-Pm4-120	38.5	28.7	100	18.8	6.7	98.9	**1.34**
T85-3-Pm3-120	27.5	28.1	100	23.2	6.1	94.9	**0.98**
T85-3-Pm2-120	22.8	27.3	100	19.2	6.1	90.0	**0.84**
T85-3-Pm1-120	20.2	24.2	100	20.4	6.5	87.9	**0.83**
T85-3-Se1-120	14.3	27.2	100	29.3	15.1	95.4	**0.53**
T80-3-Se1-120	17.3	25.4	100	21.7	13.9	91.5	**0.68**
T75-3-Se1-120	7.8	43.7	100	48.6	10.6	108.2	**0.18**
T50-3-Se1-120	5.2	47.7	100	63.0	13.3	117.7	**0.11**
T25-3-Se1-120	17.1	26.8	100	26.2	13.6	94.3	**0.64**
C300	16.0	47.6	100	27.4	3.8	100.0	**0.34**

Note: %Crystallinity was based on Eq. 1.

3.5. TGA analyses

The HKUST-1 ($Cu_3(BTC)_2(H_2O)_3 \cdot xH_2O$, x≈3) was tested in TGA to show its thermal stability. As shown in Fig. 6, these samples have similar TG curves from 35 to 900°C. At temperatures below 120°C, the weight loss is due to the desorption of physisorbed water or gases. This was followed by the release of water trapped in the pores when the temperature was raised up to 180°C. The HKUST-1 was then heated up to 350°C and exhibited modest loss of weight, as shown in DTG curve of the Fig. 6. However, the weight loss increased significantly when temperature was raised above 350°C. At higher temperatures, some metal were reduced and MOFs were decomposed to form carbon. The weight loss levelled off at higher temperatures when MOFs were completely transformed into CO_2, CO, Cu, Cu_2O, and CuO. This finding is consistent with what has been reported by others, the MOFs retained its molecular formula but lost the microporous nature after being heated to 350 to 427°C [43].

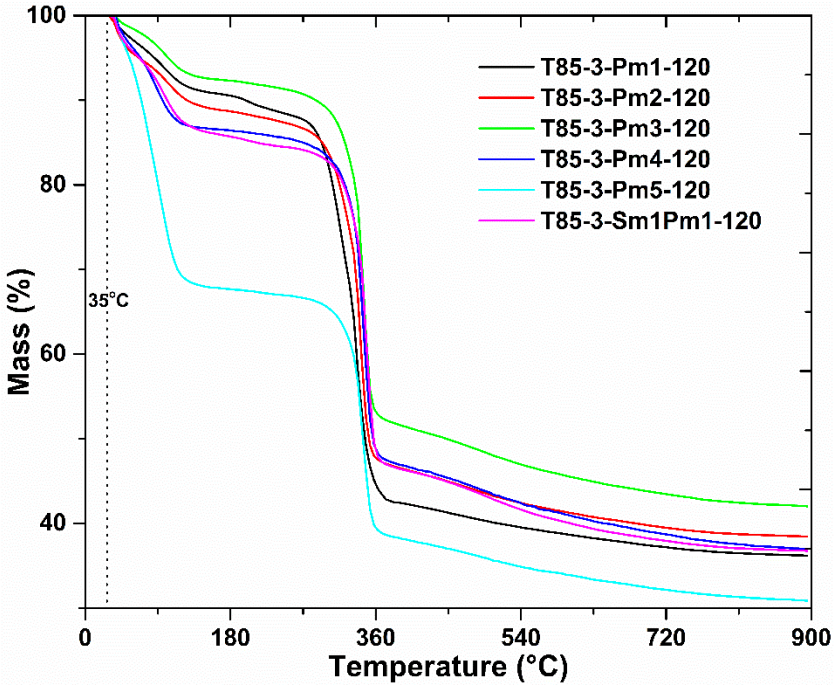

Fig. 6 TGA analysis of T85-3A-Pm1, Pm2, Pm3, Pm4, Pm5 and Sm1Pm1-120 from 35°C to 900°C within N_2 atmosphere.

3.6. CO_2 adsorption analyses

It was found that the presence of divalent metals significantly increased CO_2 binding strength and resulted in higher selectivity in CO_2 adsorption [44]. Due to its crystalline structure and the existence of Cu^{2+} metal ions, HKUST-1 is expected to have high affinity toward CO_2. Normally, CO_2 adsorption can be evaluated by two methods, i.e., static and dynamic adsorption. In this study, the static adsorption test was carried out at 27°C with pressure from 0-1bar. In the dynamic test, a thermogravimetric study using pure CO_2 was carried out at 27°C.

The CO_2 uptake of T85-3-Pm**X**-120 (X=1,2,3,4,5) and T85-3-Sm1Pm**1**-120 is shown in Fig. 7. The CO_2 uptake capacity of T85-3-Pm4-120 sample exhibits a steep rise in a short time, and reach a maximum of 8.12% wt. (1.84 mmol/g), at 27°C and 1 bar. It is generally believed that CO_2 adsorption capacity is dependent on pore volume of the adsorbent[45]. The larger the microporosity, the higher the CO_2 adsorption capacity. Besides, the I_{200}/I_{220} ratio of each sample can be used as an indicator for CO2 adsorption capacity.

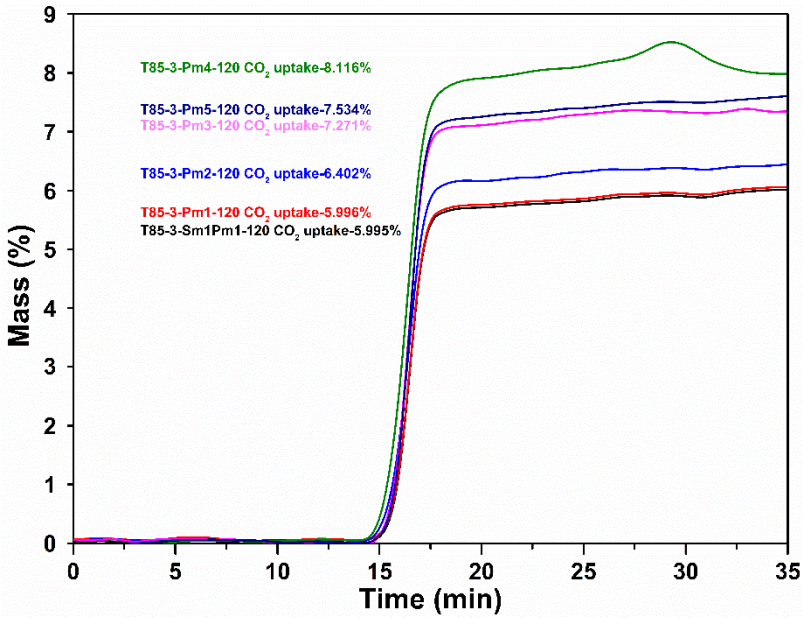

Fig. 7 Adsorption capacity of CO_2 at 27°C for HKUST-1 samples (TGA data)

To reveal the CO_2 adsorption property of T85-3-Pm4-120, CO_2 adsorption isotherm was obtained and is shown in Fig. 8. The CO_2 recycle of T85-3-Pm4-120 was measured at 27°C under 1 bar. The results showed that the CO_2 desorption process finished rapidly during N_2 purging under the same conditions and the CO_2 adsorption capacity remains almost unchanged after ten adsorption/desorption cycles, which demonstrated the good adsorption stability of T85-3-Pm4-120. It is clear that T85-3-Pm4-120 has a CO_2 uptake of 11 wt% (2.5mmol/g) under static adsorption, which is higher than reported data under similar experimental conditions as shown in Table 4.

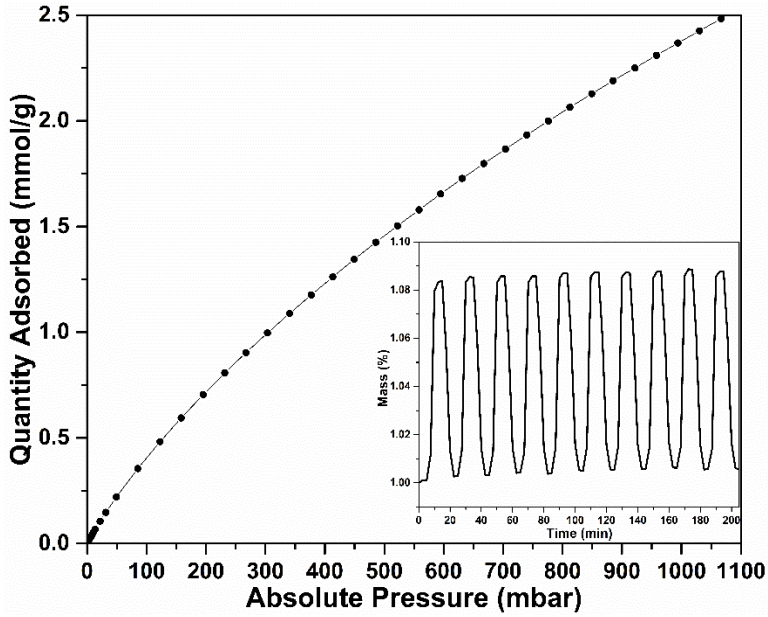

Fig. 8 CO_2 isotherm of T85-3-Pm4-120 at 27°C, inset graph is CO_2 recycle of T85-3-Pm4-120

Table 4 Comparison of CO_2 adsorption capacity for others' HKUST-1

Literature	Adsorption manner	Adsorption capacity mmol/g	Adsorption temperature ^{o}C
Sheng et al. [46]	Dynamic adsorption	1.82	30
Chugh et al. [47]	Dynamic adsorption	1.45	30
Shen et al. [48]	Static adsorption	0.15	20 (0.75 bar)
Yunxia et al. [49]	Dynamic adsorption	1.8	32 (5 bar)
This research	Dynamic adsorption	1.84	27 (1 bar)
This research	Static adsorption	1.95	27 (0.75 bar)
This research	Static adsorption	2.5	27 (1 bar)

4. Conclusions

In conclusion, the optimized hydro/solvo-thermal approach developed in this research is a cheap and efficient method for the synthesis of nanoscale HKUST-1 MOFs under low temperature and atmospheric pressure using methanol as the activation agent. Both the slurry and powder state

368 activation methods were found to have significant influence on the specific surface area,
369 micropore volume and mesopore size, while powder state activation is more effective in the
370 removal of impurities trapped in HKUST-1. The **T85-3-Pm4-120** showed a high BET surface area
371 of 1542.4m^2/g and an average size of 87 nm. It was also found that the HKUST-1 prepared in this
372 study showed a high CO_2 adsorption capacity with an uptake around 11wt% (2.5mmol/g) at 27^oC
373 and 1 bar.

374 **Acknowledgement**

375 Following funding bodies are acknowledged for partially sponsoring this research: National Key
376 R&D Program of China (2017YFB0602602 and 2017YFC0210400). The University of Nottingham
377 Ningbo China is also acknowledged for the provision of full scholarship to the first two authors.
378 Authors 1 and 2 contributed equally to this work.
379

Reference

1. Farrusseng, D., *Metal-organic frameworks: applications from catalysis to gas storage*. John Wiley & Sons: 2011.

2. Wee, L. H.; Bajpe, S. R.; Janssens, N.; Hermans, I.; Houthoofd, K.; Kirschhock, C. E.; Martens, J. A., Convenient synthesis of Cu3(BTC)2 encapsulated Keggin heteropolyacid nanomaterial for application in catalysis. *Chem Commun (Camb)* **2010,** *46* (43), 8186-8.

3. Jiang, D.; Mallat, T.; Krumeich, F.; Baiker, A., Polymer-assisted synthesis of nanocrystalline copper-based metal–organic framework for amine oxidation. *Catalysis Communications* **2011,** *12* (7), 602-605.

4. Tanaka, D.; Henke, A.; Albrecht, K.; Moeller, M.; Nakagawa, K.; Kitagawa, S.; Groll, J., Rapid preparation of flexible porous coordination polymer nanocrystals with accelerated guest adsorption kinetics. *Nat Chem* **2010,** *2* (5), 410-416.

5. Beg, S.; Rahman, M.; Jain, A.; Saini, S.; Midoux, P.; Pichon, C.; Ahmad, F. J.; Akhter, S., Nanoporous metal organic frameworks as hybrid polymer-metal composites for drug delivery and biomedical applications. *Drug Discov Today* **2017,** *22* (4), 625-637.

6. Vishnyakov, A.; Ravikovitch, P. I.; Neimark, A. V.; Bülow, M.; Wang, Q. M., Nanopore structure and sorption properties of Cu− BTC metal− organic framework. *Nano Letters* **2003,** *3* (6), 713-718.

7. Chui, S. S.-Y.; Lo, S. M.-F.; Charmant, J. P.; Orpen, A. G.; Williams, I. D., A chemically functionalizable nanoporous material [Cu3 (TMA) 2 (H2O) 3] n. *Science* **1999,** *283* (5405), 1148-1150.

8. Biemmi, E.; Christian, S.; Stock, N.; Bein, T., High-throughput screening of synthesis parameters in the formation of the metal-organic frameworks MOF-5 and HKUST-1. *Microporous and Mesoporous Materials* **2009,** *117* (1-2), 111-117.

9. Yaghi, O. M.; O'Keeffe, M.; Ockwig, N. W.; Chae, H. K.; Eddaoudi, M.; Kim, J., Reticular synthesis and the design of new materials. *Nature* **2003,** *423* (6941), 705-714.

10. Férey, G.; Mellot-Draznieks, C.; Serre, C.; Millange, F., Crystallized Frameworks with Giant Pores: Are There Limits to the Possible? *Accounts of Chemical Research* **2005,** *38* (4), 217-225.

11. Kitagawa, S.; Kitaura, R.; Noro, S., Functional porous coordination polymers. *Angew Chem Int Ed Engl* **2004,** *43* (18), 2334-75.

12. Ferey, G., Hybrid porous solids: past, present, future. *Chem Soc Rev* **2008,** *37* (1), 191-214.

13. Stock, N.; Biswas, S., Synthesis of metal-organic frameworks (MOFs): routes to various MOF topologies, morphologies, and composites. *Chem Rev* **2012,** *112* (2), 933-69.

14. Chaturvedi, S.; Dave, P. N.; Shah, N. K., Applications of nano-catalyst in new era. *Journal of Saudi Chemical Society* **2012,** *16* (3), 307-325.

15. Yang, Q.; Li, C., Catalysis in Porous - Material - Based Nanoreactors: a Bridge between Homogeneous and Heterogeneous Catalysis. *Bridging Heterogeneous And Homogeneous Catalysis: Concepts, Strategies, And Applications*, 351-396.

16. Lestari, W. W.; Arvinawati, M.; Martien, R.; Kusumaningsih, T., Green and facile synthesis of MOF and nano MOF containing zinc(II) and benzen 1,3,5-tri carboxylate and its study in ibuprofen slow-release. *Materials Chemistry and Physics* **2018,** *204*, 141-146.

17. Wahiduzzaman; Allmond, K.; Stone, J.; Harp, S.; Mujibur, K., Synthesis and Electrospraying of Nanoscale MOF (Metal Organic Framework) for High-Performance CO2 Adsorption Membrane. *Nanoscale Research Letters* **2017,** *12* (1), 6.

18. Li, P.; Klet, R. C.; Moon, S. Y.; Wang, T. C.; Deria, P.; Peters, A. W.; Klahr, B. M.; Park, H. J.; Al-Juaid, S. S.; Hupp, J. T.; Farha, O. K., Synthesis of nanocrystals of Zr-based metal-organic frameworks with csq-net: significant enhancement in the degradation of a nerve agent simulant. *Chem Commun (Camb)* **2015,** *51* (54), 10925-8.

19. Khan, N. A.; Jhung, S.-H., Facile Syntheses of Metal-organic Framework Cu3(BTC)2(H2O)3under Ultrasound. *Bulletin of the Korean Chemical Society* **2009,** *30* (12), 2921-2926.

20. Schlesinger, M.; Schulze, S.; Hietschold, M.; Mehring, M., Evaluation of synthetic methods for microporous metal–organic frameworks exemplified by the competitive formation of [Cu2(btc)3(H2O)3] and [Cu2(btc)(OH)(H2O)]. *Microporous and Mesoporous Materials* **2010,** *132* (1-2), 121-127.

21. Kim, J.; Kim, S.-H.; Yang, S.-T.; Ahn, W.-S., Bench-scale preparation of Cu 3 (BTC) 2 by ethanol reflux: Synthesis optimization and adsorption/catalytic applications. *Microporous and Mesoporous Materials* **2012,** *161*, 48-55.

22. Lee, Y.-R.; Kim, J.; Ahn, W.-S., Synthesis of metal-organic frameworks: A mini review. *Korean Journal of Chemical Engineering* **2013,** *30* (9), 1667-1680.

23. Zhao, H.; Yang, G.; Gao, X.; Pang, C. H.; Kingman, S. W.; Wu, T., Hg(0) Capture over CoMoS/gamma-Al2O3 with MoS2 Nanosheets at Low Temperatures. *Environ Sci Technol* **2016,** *50* (2), 1056-64.

24. Yao, Q.; Su, J.; Zou, X., SUMOF-5: a mesoporous metal-organic framework with the tbo topology built from the dicopper paddle-wheel cluster and a new tritopic linker. *Zeitschrift für Kristallographie - Crystalline Materials* **2013,** *228* (7), 323-329.

25. Blanco-Brieva, G.; Campos-Martin, J. M.; Al-Zahrani, S. M.; Fierro, J. L. G., Efficient solvent regeneration of Basolite C300 used in the liquid-phase adsorption of dibenzothiophene. *Fuel* **2013,** *113*, 216-220.

26. Majchrzak-Kucęba, I.; Bukalak-Gaik, D., Regeneration performance of metal–organic frameworks. *Journal of Thermal Analysis and Calorimetry* **2016,** *125* (3), 1461-1466.

27. Kim, H. R.; Yoon, T.-U.; Kim, S.-I.; An, J.; Bae, Y.-S.; Lee, C. Y., Beyond pristine MOFs: carbon dioxide capture by metal–organic frameworks (MOFs)-derived porous carbon materials. *RSC Advances* **2017,** *7* (3), 1266-1270.

28. Xin, C.; Zhan, H.; Huang, X.; Li, H.; Zhao, N.; Xiao, F.; Wei, W.; Sun, Y., Effect of various alkaline agents on the size and morphology of nano-sized HKUST-1 for CO2adsorption. *RSC Adv.* **2015,** *5* (35), 27901-27911.

29. Bae, J.; Choi, J. S.; Hwang, S.; Yun, W. S.; Song, D.; Lee, J.; Jeong, N. C., Multiple Coordination Exchanges for Room-Temperature Activation of Open-Metal Sites in Metal-Organic Frameworks. *ACS Appl Mater Interfaces* **2017,** *9* (29), 24743-24752.

30. Ye, S.; Jiang, X.; Ruan, L.-W.; Liu, B.; Wang, Y.-M.; Zhu, J.-F.; Qiu, L.-G., Post-combustion CO 2 capture with the HKUST-1 and MIL-101 (Cr) metal–organic frameworks: adsorption, separation and regeneration investigations. *Microporous and Mesoporous Materials* **2013,** *179*, 191-197.

31. Klimakow, M.; Klobes, P.; Thünemann, A. F.; Rademann, K.; Emmerling, F., Mechanochemical Synthesis of Metal−Organic Frameworks: A Fast and Facile Approach toward Quantitative Yields and High Specific Surface Areas. *Chemistry of Materials* **2010,** *22* (18), 5216-5221.

32. Li, L.; Liu, X. L.; Gao, M.; Hong, W.; Liu, G. Z.; Fan, L.; Hu, B.; Xia, Q. H.; Liu, L.; Song, G. W.; Xu, Z. S., The adsorption on magnetic hybrid Fe3O4/HKUST-1/GO of methylene blue from water solution. *J. Mater. Chem. A* **2014,** *2* (6), 1795-1801.

33. Fang, Z.; Dürholt, J. P.; Kauer, M.; Zhang, W.; Lochenie, C.; Jee, B.; Albada, B.; Metzler-Nolte, N.; Pöppl, A.; Weber, B.; Muhler, M.; Wang, Y.; Schmid, R.; Fischer, R. A., Structural Complexity in Metal–Organic Frameworks: Simultaneous Modification of Open Metal Sites and Hierarchical Porosity by Systematic Doping with Defective Linkers. *Journal of the American Chemical Society* **2014,** *136* (27), 9627-9636.

34. Thommes, M., Physical Adsorption Characterization of Nanoporous Materials. *Chemie Ingenieur Technik* **2010,** *82* (7), 1059-1073.

35. Jang, H. R.; Oh, H.-J.; Kim, J.-H.; Jung, K. Y., Synthesis of mesoporous spherical silica via spray pyrolysis: Pore size control and evaluation of performance in paclitaxel pre-purification. *Microporous and Mesoporous Materials* **2013,** *165*, 219-227.

36. Park, J. T.; Roh, D. K.; Patel, R.; Kim, E.; Ryu, D. Y.; Kim, J. H., Preparation of TiO2 spheres with hierarchical pores via grafting polymerization and sol–gel process for dye-sensitized solar cells. *Journal of Materials Chemistry* **2010,** *20* (39), 8521.

37. Diring, S.; Furukawa, S.; Takashima, Y.; Tsuruoka, T.; Kitagawa, S., Controlled multiscale synthesis of porous coordination polymer in nano/micro regimes. *Chemistry of Materials* **2010,** *22* (16), 4531-4538.

38. Ameloot, R.; Gobechiya, E.; Uji‐i, H.; Martens, J. A.; Hofkens, J.; Alaerts, L.; Sels, B. F.; De Vos, D. E., Direct patterning of oriented metal–organic framework crystals via control over crystallization kinetics in clear precursor solutions. *Advanced materials* **2010,** *22* (24), 2685-2688.

39. Schlesinger, M.; Schulze, S.; Hietschold, M.; Mehring, M., Evaluation of synthetic methods for microporous metal–organic frameworks exemplified by the competitive formation of [Cu 2 (btc) 3 (H 2 O) 3] and [Cu 2 (btc)(OH)(H 2 O)]. *Microporous and Mesoporous Materials* **2010,** *132* (1), 121-127.

40. Liu, J.; Culp, J. T.; Natesakhawat, S.; Bockrath, B. C.; Zande, B.; Sankar, S.; Garberoglio, G.; Johnson, J. K., Experimental and theoretical studies of gas adsorption in Cu3 (BTC) 2: an effective activation procedure. *The Journal of Physical Chemistry C* **2007,** *111* (26), 9305-9313.

41. Yakovenko, A. A.; Reibenspies, J. H.; Bhuvanesh, N.; Zhou, H.-C., Generation and applications of structure envelopes for porous metal–organic frameworks. *Journal of Applied Crystallography* **2013,** *46* (2), 346-353.

42. He, X.; Gan, Z.; Fisenko, S.; Wang, D.; El-Kaderi, H. M.; Wang, W. N., Rapid Formation of Metal-Organic Frameworks (MOFs) Based Nanocomposites in Microdroplets and Their Applications for CO2 Photoreduction. *ACS Appl Mater Interfaces* **2017,** *9* (11), 9688-9698.

43. Huang, L.; Joshi, K. L.; van Duin, A. C.; Bandosz, T. J.; Gubbins, K. E., ReaxFF molecular dynamics simulation of thermal stability of a Cu 3 (BTC) 2 metal–organic framework. *Physical Chemistry Chemical Physics* **2012,** *14* (32), 11327-11332.

44. Dauth, A.; Love, J. A., Synthesis and reactivity of 2-azametallacyclobutanes. *Dalton Trans* **2012,** *41* (26), 7782-91.

45. Liu, S.-H.; Lin, Y.-C.; Chien, Y.-C.; Hyu, H.-R., Adsorption of CO2 from Flue Gas Streams by a Highly Efficient and Stable Aminosilica Adsorbent. *Journal of the Air & Waste Management Association* **2011,** *61* (2), 226-233.

46. Ye, S.; Jiang, X.; Ruan, L.-W.; Liu, B.; Wang, Y.-M.; Zhu, J.-F.; Qiu, L.-G., Post-combustion CO2 capture with the HKUST-1 and MIL-101(Cr) metal–organic frameworks: Adsorption, separation and regeneration investigations. *Microporous and Mesoporous Materials* **2013,** *179*, 191-197.

47. Chugh, R.; Bajpai, P.; Bhunia, H. Carbon dioxide adsorption on metal organic framework Basolite C300. 2015.

48. Aprea, P.; Caputo, D.; Gargiulo, N.; Iucolano, F.; Pepe, F., Modeling carbon dioxide adsorption on microporous substrates: comparison between Cu-BTC metal− organic framework and 13X zeolitic molecular sieve. *Journal of Chemical & Engineering Data* **2010,** *55* (9), 3655-3661.

49. Zhao, Y.; Cao, Y.; Zhong, Q., CO2 Capture on Metal-Organic Framework and Graphene Oxide Composite Using a High-Pressure Static Adsorption Apparatus. *Journal of Clean Energy Technologies* **2014**, 34-37.